DEVELOPMENT OF ADVANCED PROPAGATION MODELS AND APPLICATION TO THE STUDY OF IMPULSIVE INFRASONIC EVENTS

David E. Norris[1], Joydeep Bhattacharyya[1], and Rodney W. Whitaker[2]

BBN Technologies[1] and Los Alamos National Laboratory[2]

Sponsored by Army Space and Missile Defense Command

Contract No. W9113M-05-C-0135

ABSTRACT

Research advances have been made in the areas of advanced model development, ground truth (GT) event studies, and model validation. They are focused on understanding the driving mechanisms that affect measured waveforms, and quantifying the prediction performance of new modeling capabilities. High fidelity predictions of infrasonic waveforms properties, including travel time and amplitude, improve source localization. These advances also support discrimination between various infrasonic impulsive events.

New additions have been made to the GT database. These additions mainly focus on events that are directly related to nuclear weapons testing: near-surface nuclear explosion (NE), underground nuclear explosion (UNE), and high-explosives (HE) events. They are well-calibrated GT events and significant domain knowledge resides with our Los Alamos National Laboratory (LANL) colleagues. Digital waveforms from the HE events at range of 1.5 to 60 km have been acquired and will be used to explore the boundaries between propagation regimes near the infrasound source.

New propagation modeling capabilities include a ray model that incorporates the effects of diffraction, PE/TDPE models that incorporate small-scale atmospheric variability, and PE/TDPE models that account for terrain. Detailed model comparisons studies have been complete for both the 1988 Henderson explosion and White Sands Missile Range (WSMR) I, II, and III rocket experiments.

Report Documentation Page

Form Approved
OMB No. 0704-0188

1. REPORT DATE	2. REPORT TYPE	3. DATES COVERED
SEP 2007		**00-00-2007 to 00-00-2007**

4. TITLE AND SUBTITLE	5a. CONTRACT NUMBER
Development of Advanced Propagation Models and Application to the Study of Impulsive Infrasonic Events	5b. GRANT NUMBER
	5c. PROGRAM ELEMENT NUMBER
6. AUTHOR(S)	5d. PROJECT NUMBER
	5e. TASK NUMBER
	5f. WORK UNIT NUMBER
7. PERFORMING ORGANIZATION NAME(S) AND ADDRESS(ES) **Los Alamos National Laboratory,PO Box 1663,Los Alamos,NM,87545**	8. PERFORMING ORGANIZATION REPORT NUMBER
9. SPONSORING/MONITORING AGENCY NAME(S) AND ADDRESS(ES)	10. SPONSOR/MONITOR'S ACRONYM(S)
	11. SPONSOR/MONITOR'S REPORT NUMBER(S)

12. DISTRIBUTION/AVAILABILITY STATEMENT
Approved for public release; distribution unlimited

13. SUPPLEMENTARY NOTES
Proceedings of the 29th Monitoring Research Review: Ground-Based Nuclear Explosion Monitoring Technologies, 25-27 Sep 2007, Denver, CO sponsored by the National Nuclear Security Administration (NNSA) and the Air Force Research Laboratory (AFRL)

14. ABSTRACT
see report

15. SUBJECT TERMS

16. SECURITY CLASSIFICATION OF:			17. LIMITATION OF ABSTRACT	18. NUMBER OF PAGES	19a. NAME OF RESPONSIBLE PERSON
a. REPORT **unclassified**	b. ABSTRACT **unclassified**	c. THIS PAGE **unclassified**	**Same as Report (SAR)**	**10**	

OBJECTIVES

The objectives for this research contract are twofold. The first objective involves developing advancements in propagation modeling capabilities: a PE model accounting for ambient density gradients, a ray model that includes the effects of diffraction, and PE and TDPE models that account for variable terrain and fine-scale atmospheric structure. The second objective involves identifying and compiling ground truth data sets and using them for event analysis and model comparison studies.

Through these efforts, some of the driving mechanisms affecting the measured waveforms will be identified, and the prediction performance of the new models will be quantified. These advances will ultimately improve event localization capabilities. More robust prediction of infrasonic arrivals, for example, those that reach the ground through diffraction, more accurate travel-time predictions, and more robust amplitude predictions will improve localization. In addition, these advances will support discrimination between various infrasonic impulsive events.

RESEARCH ACCOMPLISHED

Ray Diffraction

A significant limitation to standard ray theory occurs when shadow zones are present. Shadow zones are regions where no rays penetrate and zero amplitude is predicted. They form between ground bounces and below elevated ducts. Despite ray theory predictions, acoustic energy can reach into shadow zones through diffraction and scattering (Gilbert and Raspet, 1990).

We have extended the capabilities of ray tracing by integrating a ray diffraction model for application to the boundary of elevated ducts. The modeling approach is based on identifying a diffraction region and propagating the diffracted ray from this point down to the receiver. The travel time is computed over the total ray path from the source to the diffraction region and from the diffraction region to the receiver.

As an example, consider the April 23, 2001, north pacific bolide that was observed at a multitude of stations, including IS57 in Pinon Flats, California. Figure 1 shows a fan of rays computed from the source region along the bearing to IS57. All these rays are trapped in an elevated stratospheric duct. However, observations suggest a signal velocity (range over travel time) more consistent with a stratospheric path than a thermospheric one. This arrival may result from energy leaking out of the elevated stratospheric duct.

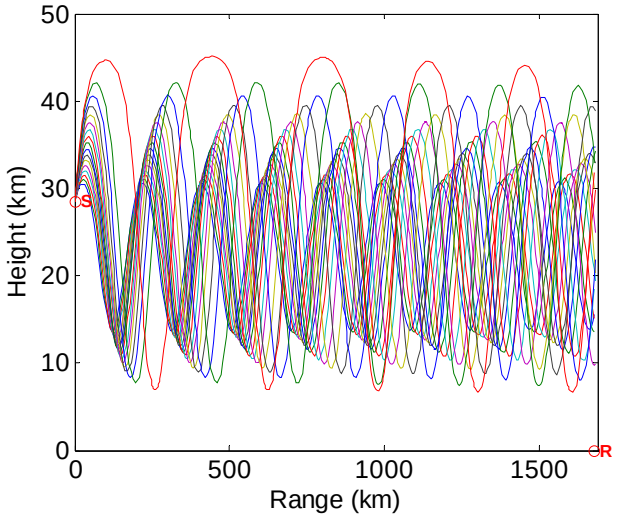

Figure 1. Stratospheric rays from the April 23, 2001, Pacific bolide to IS57.

To test this hypothesis, a diffracted ray is computed off of the lower turning height region for a representative ray. This region is approximately 50 km short in range from the receiver. The representative and diffracted rays are shown in Figure 2. The total travel time from source to receiver over this path is 5653 s. The observed arrival time spans a range from 5608 to 6298 s, with a peak energy at 5953 s. The predicted arrival time falls within this range and differs from the peak arrival by 5%. This comparison supports the hypothesis that IS57 observed diffracted stratospheric energy.

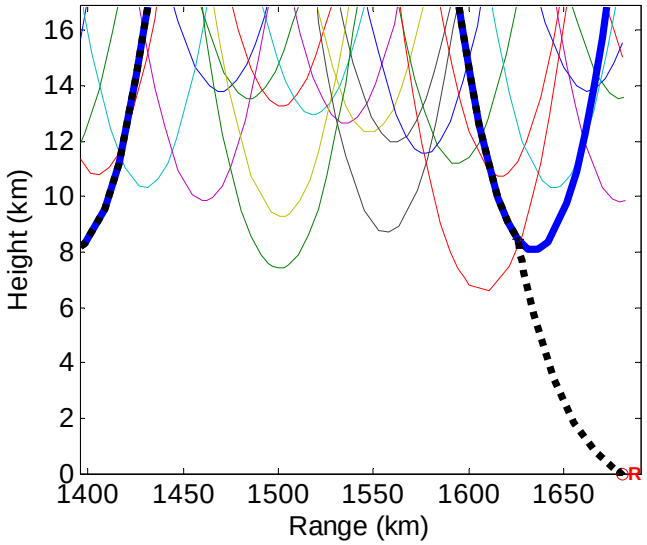

Figure 2. Stratospheric rays near the receiver, showing ray with lower turning height of 8 km (blue) and diffracted ray (dotted black).

Ground Truth Database

We have continued to expand our GT database by focusing on events that are directly related to the nuclear weapons testing, e.g., near-surface and underground nuclear explosions and HE events. These are well-calibrated, man-made events and significant domain knowledge resides with our LANL colleagues.

Underground nuclear explosions

Los Alamos National Laboratory has operated infrasound arrays in Nevada, New Mexico, and Utah since the early 1980s. These were mostly four-element arrays, with three sensors arranged in a triangle and the fourth at the center. In some cases, seismic data were also recorded at the same sites. Over the years, these arrays have recorded a variety of acoustic events, including UNEs at the Nevada Test Site (NTS) and subsequent cavity collapses, and conventional explosions both above and below ground.

Near-surface nuclear explosions

We have obtained digital waveform data for the near surface nuclear explosions from Operation Teapot carried out in the spring of 1955 from Eric Chael of Sandia National Laboratories (SNL) (Chael, 2004). This series includes several events with yields from 1 kt to 43 kt, all detonated a few hundred feet above ground. Table 1 lists the events for which we have digital records from these series of tests. Chael has extracted about 15 traces per test from the available stations, some of which used two sensors separated about 1 mile along the direction from NTS. For the larger events, detected signals are distinct at frequencies between 0.5–3.0 Hz; for the smaller events (<20 kt), higher frequencies are observed (Chael, 2004). We have separately contacted Jack Reed (currently retired) to obtain the station locations and have been successful in extracting accurate locations from his private archives.

Table 1. Near-surface nuclear explosions with available digital waveforms.

Event Name	Date	Time	Location	Latitude (°N)	Longitude (°E)	Height (km)	Size (kT)
Yankee	05/04/54	18:10:00	Bikini	11.6655	165.3869	N/A	13500
Wasp	02/18/55	19:59:59	NTS	37.0867	-116.0219	0.2	1
Turk	03/07/55	13:20:00	NTS	37.1383	-116.1175	0.2	43
Hornet	03/12/55	13:20:00	NTS	37.0403	116.0253	0.1	4
Bee	03/22/55	13:05:00	NTS	37.0947	-116.0239	0.2	4
Ess	03/23/55	20:30:00	NTS	37.1683	-116.0439	0	1
Wasp Prime	03/29/55	17:59:55	NTS	37.0867	-116.0578	0.2	3
HA	04/06/55	18:00:04	NTS	37.0286	-116.0578	11.2	3

Near-surface high-explosives events

Controlled HE field tests can be some of the best infrasonic sources for validating propagation models at local to near-regional distances. Much of our current knowledge of infrasound generated by explosions is a results of the HE tests made at the WSMR by the Defense Nuclear Agency (DNA). The DNA HE shots were a series of chemical explosions during the 1980s and early 1990s. Currently, we have obtained the source location, source size, event time, and station locations for several of the HE events. The times are accurate to milliseconds and the locations are accurate to about 10 m.

We have obtained digital waveform data files for Distant Image and Minor Uncle, and paper records for Miser's Gold. The digital data were recorded with 3-channel Terra Tech 12-bit tape recorders sampling at 200 Hz. Channels 1 and 2 for all these files are vertical and radial seismic and Channel 3 is pressure recorded with the Validyne gages in pascals. Though no hose arrays were used for wind noise reduction, just an open port about 16 inches off the ground, the data at distances less than 60 km have good signal-to-noise ratios (SNR). Figure 3 gives an example digital waveform recorded during the Minor Uncle test.

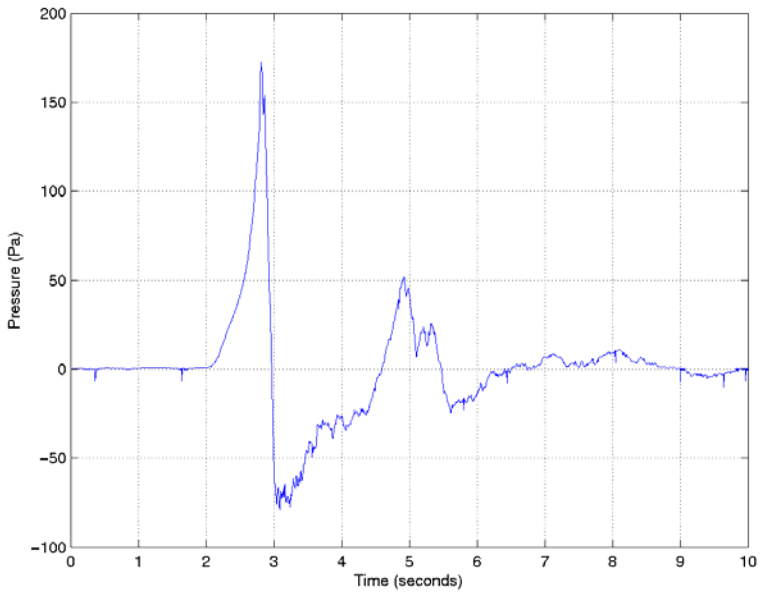

Figure 3. Minor Uncle infrasound signal measured at San Antonio, NM, at a range of approximately 50 km.

For each of the HE shots, we have access to infrasound recordings at a set of single component stations. Figure 4 shows some of the waveforms for the Distant Image event. Along with infrasound waveforms, our near-source HE data set includes seismic waveforms that might be used for seismo-acoustic studies critical to nuclear explosion monitoring. Figure 5 shows the digital recordings of co-located seismic and infrasound waveforms.

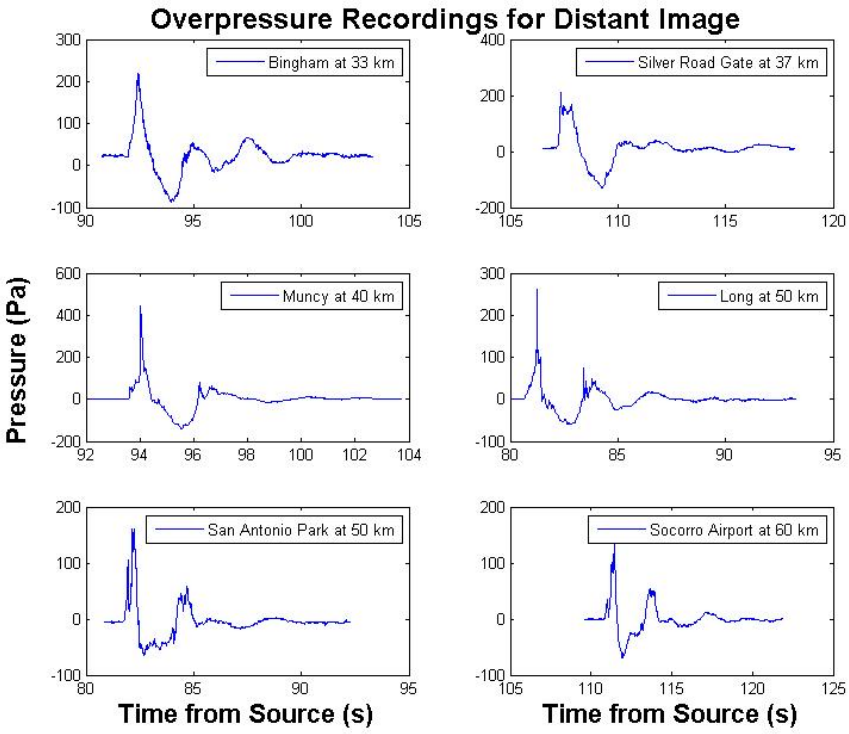

Figure 4. Infrasound waveforms at a set of stations for the Distant Image event.

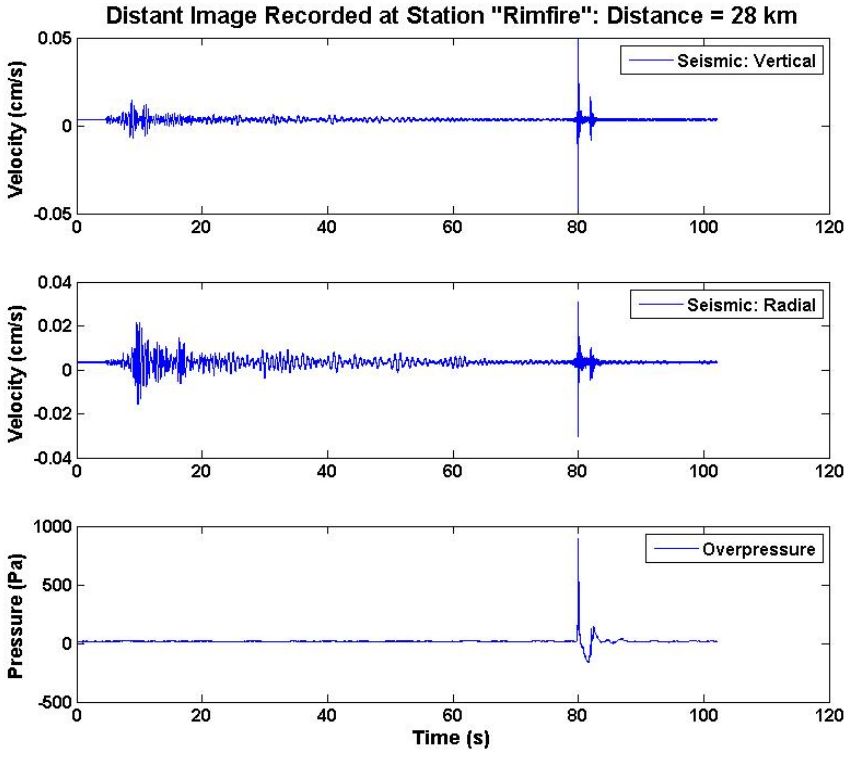

Figure 5. Seismic and infrasound waveforms from the Distant Image shot, recorded at co-located stations.

Special events from the LANL tape database

We have computer tapes at LANL that contain infrasound recordings of explosions during 1983 to 1991. We have developed MATLAB scripts that let us extract the digital waveforms and save them ASCII format. This data set includes data from the large accidental explosion that occurred at a chemical plant in Henderson, Nevada, on May 4, 1988. The tape data set also contains digital waveforms for a set of five UNEs carried out at NTS, Nevada. We are currently extracting these waveforms. Figure 6 shows the waveforms recorded at St. George, Utah, from the Texarkana event.

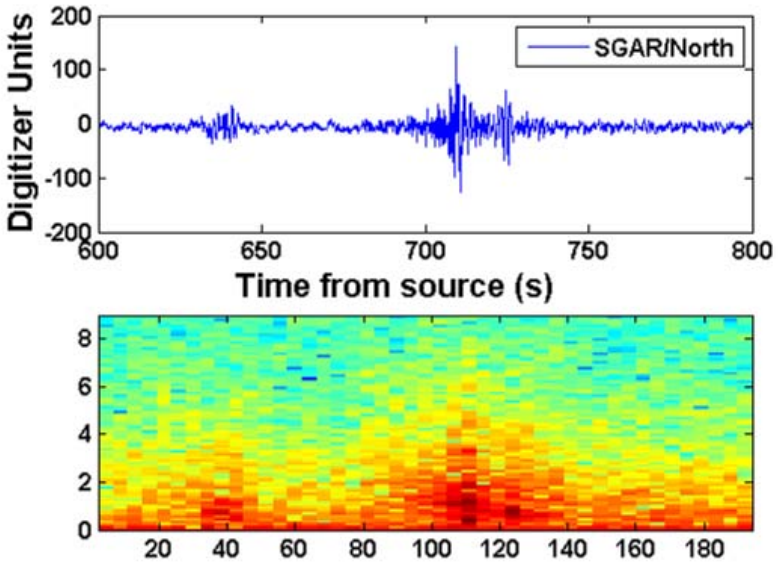

Figure 6. Recorded infrasound waveforms at one of the SGAR array elements, along with its spectrogram, from the Texarkana underground nuclear explosion of February 10, 1989.

Preliminary Analysis of Waveform Parameters Related to the WSMR Explosions

We have developed a time-domain parabolic equation (TDPE) technique to model the recorded waveforms from the WSMR explosions. Our broadband synthetic waveforms are computed for the GT source and the receiver locations published for the experiment and meteorological conditions obtained from the Naval Research Laboratory (NRL) G2S model. The TDPE synthetics are thus expected to capture realistic propagation conditions and can thus be compared to the recorded waveforms.

In this analysis, we carry out comparison studies for several parameters that define the signal from the WSMR shots recorded at several western U.S. infrasound array stations. These parameters are as follows:

- Travel time of the stratospheric propagation, using the GT source time
- The signal duration
- Dominant frequency of the signal
- RMS signal level
- Signal velocity, derived from source and receiver location and the travel time

We carry out an interactive analysis to estimate the aforementioned parameters from the data and model. This step is essential to assure quality of the measurements. We use the relationship of the signal with respect to the background noise to identify the start and end times of the waveforms, and thus the duration times can be somewhat under-predicted for low SNR signals. In our analysis, we focus on the signals between 0.5–3.0 Hz for both data and TDPE modeled waveforms.

We consider the data recorded at near-receiver ranges (nominally within 100 km) and those at regional distances along a particular profile toward the west from the explosions, namely, stations GILA, CHIR, and SAGU. This allows us to explore the propagations in the infrasound "shadow zone" and at distances close to the first bounce for stratospheric propagation. We focus on three separate explosions for this study: WSMR I Shot 1, WSMR I Shot 2, and WSMR III Shot 2. Signals from each of these events propagated well to the west, leading to clear detections to most of the stations considered in our study.

First we examine the variation of signal parameters between stations. Figure 7 shows the comparison between travel times for the three events. We note that the travel time misfits, generally, are significantly larger for stations at shorter distances. However, we do not detect a bias, positive or negative, for the travel time difference.

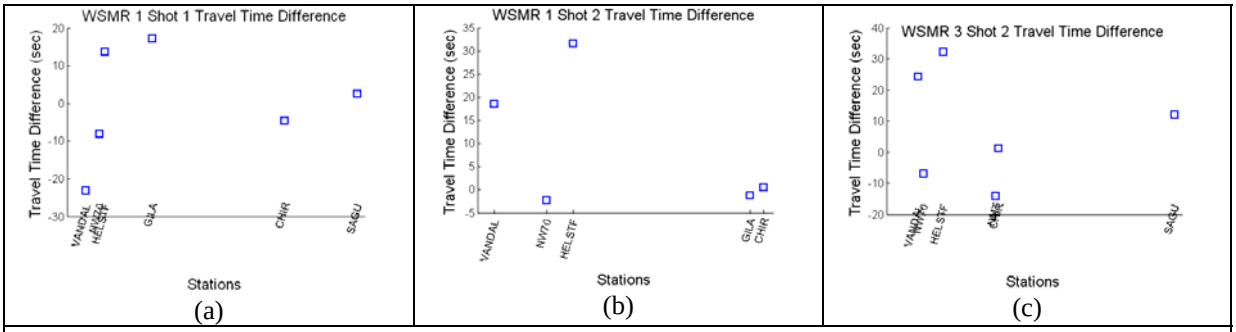

Figure 7. Difference in travel time between recorded and modeled data as a function of source-receiver distance.

Figure 8 shows a comparison between the RMS of the recorded and modeled signals. We note a consistent trend that the signal amplitudes are better predicted for the stations at farther distances. We note that the amplitude differences are comparable for most stations between the two explosions of WSMR I while they are in turn slightly larger than that of WSMR III. In nearly all of the paths, the amplitude of the recorded signal is larger than the synthetics, probably indicating that our modeling is overpredicting the signal attenuation.

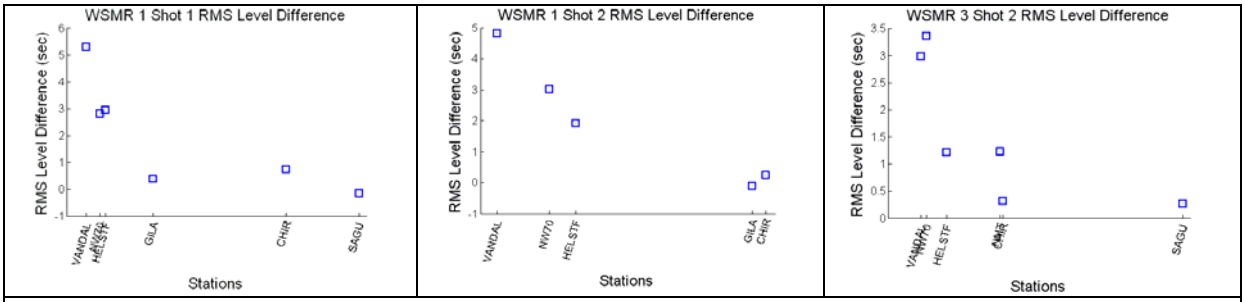

Figure 8. Comparison of RMS amplitudes of recorded and modeled signals (i.e., recorded-modeled) as a function of source-receiver distance.

Figure 9 shows a comparison of the durations between recorded and modeled signals. We note that the durations are well modeled for the close-in stations, but not for stations at further distances. As mentioned earlier, our durations are based on the visual inspection of SNR and not on array processing based detection analysis. This can lead to an under-prediction of the duration for recorded data, especially for stations at farther distances where we expect the SNR to be comparatively short. Moreover, at farther distances, there can be a significant "ringing" in our band-limited synthetics which in turn can lead to erroneous picks of signal start and end time. We are currently exploring these effects to resolve the misfits in signal duration.

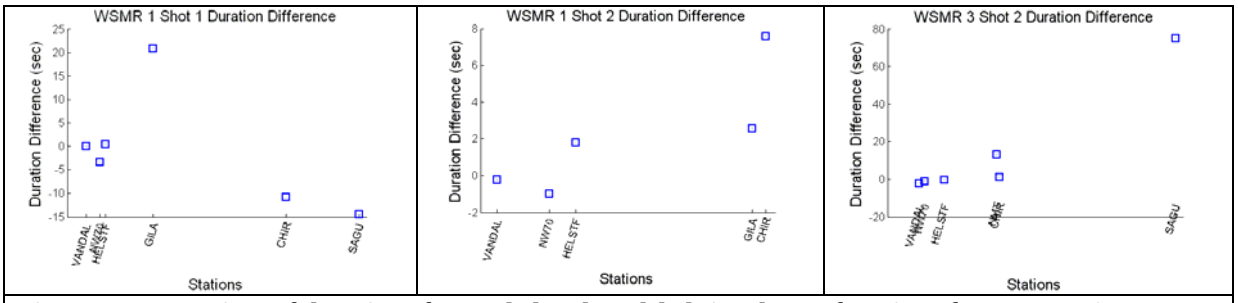

Figure 9. Comparison of duration of recorded and modeled signals as a function of source-receiver distance.

Figure 10 shows a comparison of the peak frequency of the signal. We note a trend that the peak frequencies are better modeled for stations at larger distances. Generally, we observe that the peak frequency of the data is slightly higher than that of the synthetic.

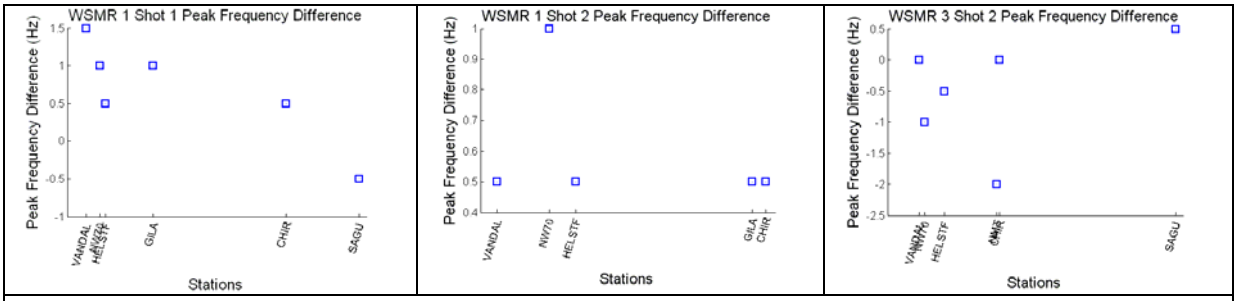

Figure 10. Comparison of peak frequencies of recorded and modeled signals as a function of source-receiver distance.

Figure 11 shows a comparison of the signal group velocity between recorded and modeled signals. Please note that we plot the actual velocity rather than the difference between those of recorded and modeled data. We note that the difference between the velocities decreases with increasing distance.

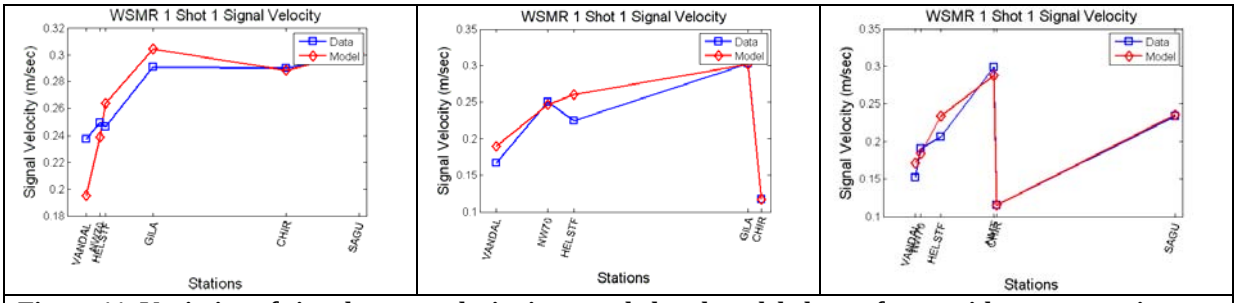

Figure 11. Variation of signal group velocity in recorded and modeled waveforms with source-receiver distance.

Now we examine the variation of signal parameter between shots. The WSMR experiments have been carried out over three separate days and covering the spring, summer and fall seasons. Moreover, there is a significant variation in altitude between the six shots involved in these experiments (Israelsson et al., 2007). Therefore, we can expect that the signal features described above can significantly differ for recordings at particular stations between the different shots. In this section, we explore the variation of some of these features, namely travel time, signal duration and amplitude, between shots and also in comparison with TDPE predictions. We focus on a subset of the stations for which the infrasonic arrivals have been clearly detected for all events and shots (Israelsson et al., 2007): VANDAL, HELSTF, and CHIR. These stations are nominally within 36 ± 10.1 km, 62 ± 10.2 km, and 292 ±1 .2 km from each of the shots, and thus represent a range of propagation environments.

Travel time

Figure 12 shows the travel times of the largest amplitude stratospheric arrival for the data and the TDPE model. Generally, we observe an increase in travel time with distance. However, we observe an anomalously large travel time, consistent between data and model, for WSMR II at CHIR. Importantly, the observed travel time can vary by up to 50 s (≈ 40% of the total travel time for WSMR I at VANDAL) for nearly identical paths propagating within several hours of each other. These results are consistent with those presented in Israelsson et al. (2007).

Figure 13 shows the difference between the observed and modeled travel times. We note that the observed waveforms for HELSTF are delayed compared to predictions. CHIR arrivals are usually early, compared to predictions, except the anomalous one for WSMR II mentioned above.

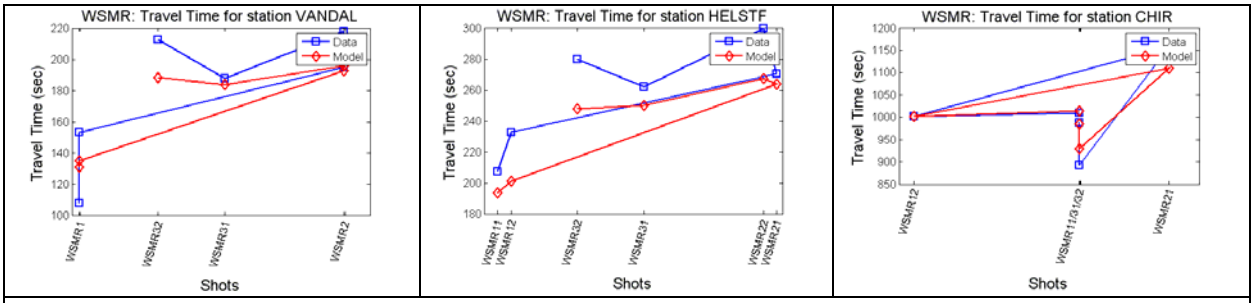

Figure 12. Observed and modeled travel times for stratospheric arrivals for all three WSMR events. The legend on the x-axis show the distance to the source and indicates both the event number (1/2/3) and shot number (1/2) within each event.

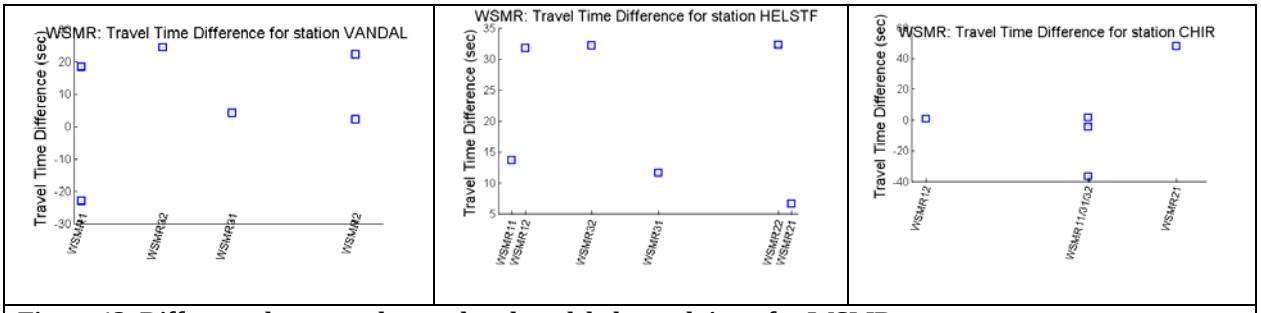

Figure 13. Difference between observed and modeled travel times for WSMR events.

Signal duration

Figure 14 shows the shot-by-shot comparison of signal duration (duration of data waveform – duration of model waveform) of the dominant stratospheric arrival. We do not observe a significant trend in our comparison of data with TDPE synthetics. However, we do note anomalously large modeled waveform duration at CHIR for WSMR II.

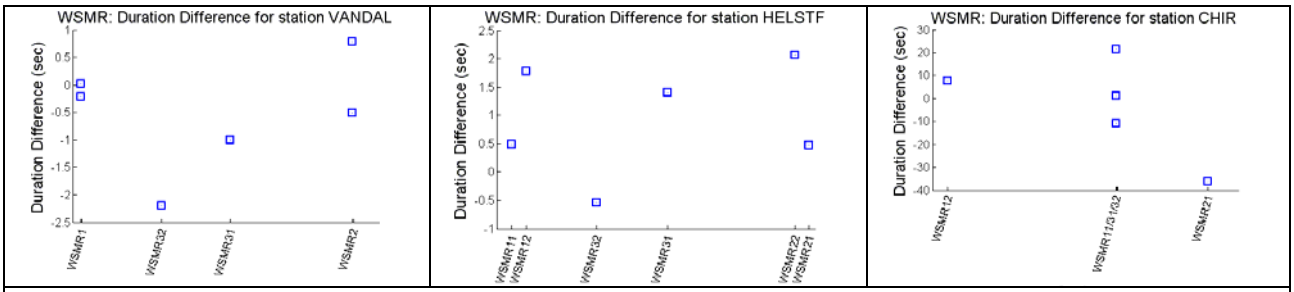

Figure 14. Observed-modeled signal duration of stratospheric arrivals for all six WSMR events.

Signal amplitude

Figure 15 shows the shot-by-shot comparison of signal amplitude, estimated using its RMS value (RMS_{data} – RMS_{model}), of the dominant stratospheric arrival. As mentioned before, the mismatch decreases with distance away from the source, and the observed amplitude is larger than the modeled one. For the closer in stations, the amplitude mismatch is largest for WSMR I and is probably related to the large source location uncertainty for these shots (Israelsson et al., 2007).

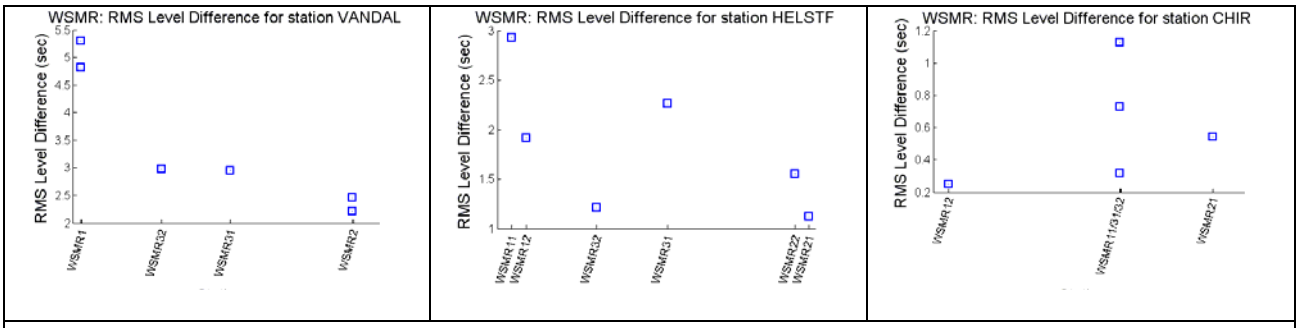

Figure 15. Observed-modeled RMS amplitude of stratospheric arrivals for all six WSMR events.

In summary we have carried out an analysis of infrasound signal parameters as recorded at a set of stations for three specific events related to the WSMR set of experiments and compare them to those predicted from infrasound propagation modeling. We note that the agreement between data and model is generally good. The misfits increases for stations lying closer to the source and indicates that possibly non-linear effects related to short-range propagation (< 100 km) might not be fully captured by our modeling technique. More realistic attenuation models will probably be required for improved waveform fits. We note significant differences in signal features misfits between different events. We are currently pursuing improvements in propagation modeling and signal picking to resolve these differences.

CONCLUSIONS AND RECOMMENDATIONS

The results of this research effort continue to advance our capabilities for accurately predicting infrasonic propagation parameters and assess the influence of fundamental physical processes. New propagation modeling capabilities include a ray diffraction model that addresses elevated ducts. Significant additions have been made to the GT database, including measurements from the DNA HE shots. In addition, preliminary comparison studies of the WSMR rocket tests are quantifying the modeling performance and areas of focus for future research.

REFERENCES

Chael, E. and R. Whitaker (2004). Infrasound signal library, in *Proceedings of the 26th Seismic Research Review: Trends in Nuclear Explosion Monitoring*, LA-UR-04-5801, Vol. 1, pp. 618–623.

Gilbert, K. and R. Raspet (1990). Calculation of turbulence effects in an upward-refracting atmosphere, *J. Acoust. Soc. Am.* 87: 2428–2437.

Israelsson, H., M. Bahavar, and R. North (2007). Source and signal summary for the WSMR infrasound experiments, SAIC report SAIC-07-2201.